Article **Journal of Technology and Innovation**

December 2023, Vol.10 No.27 8-16

Theoretical determination of histories and carbon concentration profiles in steel resulted from a thermochemical process at a frontier

Determinación teórica de historias y perfiles de concentración de carbono en acero como resultado de un proceso termoquímico desarrollándose en una frontera

TÉLLEZ-MARTÍNEZ, Jorge Sergio´*†, VEGA-FLORES, María Yaneth´, PÉREZ-QUIROZ, José Trinidad´´ and HERNÁNDEZ-MEDRANO, Verónica´´´

´Tecnológico Nacional de México / Instituto Tecnológico de Morelia, Morelia 58120, México.
´´Instituto Mexicano del Transporte, Parque Tecnológico Sanfandila, Pedro Escobedo, Querétaro C.P. 76703, México.
´´´Universidad Politécnica de Juventino Rosas. Academia de Ingeniería en Plásticos. Miguel Hidalgo 102, Comunidad de Valencia, Santa Cruz de Juventino Rosas, Gto.; México.

ID 1st Author: *Jorge Sergio, Téllez-Martínez* / **ORC ID:** 0000-0003-0587-0059, **CVU CONAHCYT ID:** 40084

ID 1st Co-author: *María Yaneth, Vega-Flores* / **ORC ID:** 0000-0002-9549-436X, **CVU CONAHCYT ID:** 1083180

ID 2nd Co-author: *José Trinidad, Pérez-Quiroz* / **ORC ID:** 0000-0002-7230-9715, **CVU CONAHCYT ID:** 91805

ID 3rd Co-author: *Verónica, Hernández-Medrano* / **ORC ID:** 0000-0002-4876-4371, **CVU CONAHCYT ID:** 751656

DOI: 10.35429/JTI.2023.27.10.8.16 Received July 15, 2023; Accepted December 30, 2023

Abstract

Steel is used to manufacture auto parts due to its properties and the ability to modify them through solid-state thermal processing. In some cases, the treated alloy itself does not satisfy the requirements of combined properties in the integrity of a single part. In these cases, thermochemical treatments do apply, with which the chemical composition does alter in a localized way. The mechanism of atomic diffusion in the solid is the mean by which atoms of a chemical element can mobilize in the lattice of the crystalline structure and concentrate, depending on the distance penetrated. The mass transport equation adequately describes concentration gradients if the diffusivity property is precisely known. The applicability to the analysis of the carburization method of steel can do a micrometric scale in one dimension. The results obtained on a computer application calculating the carbon concentration profile in iron can be shown. The strategy consists of qualitatively evaluating the distribution of equilibrium phases by optical microscopy and associating it with the carbon concentration profile.

Mass Transport, Atomic Diffusion, Carburization

Resumen

En la manufactura de autopartes se utiliza acero debido a sus propiedades y a la capacidad de modificarlas mediante procesamiento térmico en estado sólido. En algunos casos la propia aleación tratada no satisface los requerimientos de combinación de propiedades en la integridad de una parte única. Es estos casos, se recurre a los tratamientos termoquímicos con los cuales se altera la composición química de la aleación de forma localizada. El mecanismo de difusión atómica en el sólido es el medio por el cual átomos de algún elemento químico puede movilizarse en la red de la estructura cristalina y concentrarse en función de la distancia penetrada. La ecuación de transporte de masa describe adecuadamente los gradientes de concentración si se conoce con precisión la propiedad de difusividad. La aplicabilidad al análisis del método denominada carburización de aceros, puede minimizarse a sistemas en escala micrométrica en una dimensión. Como puede mostrarse, una aplicación informática que describa el perfil de concentración de carbono en hierro puede utilizarse para asociar los cálculos con el análisis metalográfico. La estrategia consistió en evaluar cualitativamente la distribución de fases de equilibrio mediante microscopia óptica y asociarla al perfil de concentración de carbono.

Transporte de Masa, Difusión Atómica, Carburización

Citation: TÉLLEZ-MARTÍNEZ, Jorge Sergio, VEGA-FLORES, María Yaneth, PÉREZ-QUIROZ, José Trinidad and HERNÁNDEZ-MEDRANO, Verónica. Theoretical determination of histories and carbon concentration profiles in steel resulted from a thermochemical process at a frontier. Journal of Technology and Innovation. 2023. 10-27:8-16.

* Correspondence of the Author (E-mail: jorge.tm@morelia.tecnm.mx)
† Researcher contributing as first author.

Introduction

The carburizing process dates back to the initially unknown technique of handcrafting swords through forging. In the evolutionary process of understanding the phenomenon, an extensive review of the theoretical foundations and industrialized processes was presented by (Edenhofer, Joritz, Rink, & Voges, 2015). His work explains that one way of executing a practice emulating ancient processes consists of imbibing a piece in a box full of powder of substances rich in carbon (pulverized charcoal, anthracite coal, or coke). The box is sealed and placed inside an oven at temperatures above 850°C for a set time. After the middle of the 20th century, salt baths and ovens with controlled gas atmospheres were used as carbon donor media.

For the processes with the carbon sources mentioned, theories of the kinetics of carbon transfer in iron and steel have been presented, the works of (Goldstein, 1978), (Grabke & Wolf, 1987), (Rahmel, Grabke, & Steinkusch, 1998), and (Grabke H. J., 2002), even address some additional topics such as the degradation effects of the substrates and the susceptibility of formation of intermetallic compounds with the alloying elements. Some approaches to mathematical models support developing computer programs for analysis (Lee, Matlock, & Van Tyne, 2013).

Modeling phenomenology

Phenomenologically, the estimation of the processing time at the carburization temperature is approximated by solving the transport equation of the carbon species (solute) in a matrix of a crystalline solid (solvent) in a transient state (Crank, 1975). Except for some cases in which assumptions about the system simplify the equation, the approach of a numerical technique is required to obtain the solution of the total field of the affected region. Therefore, when developing algorithms from specific mathematical approaches and coding them, there is the freedom to modify or implement add-ons that optimize the modeling of the system under study.

Starting from the definition that the transfer balances of chemical species in solids in terms of flow through surfaces (physical boundaries), these are developed by the law of mass transfer by diffusion or Fick's law represented by **Equation 1** (Porter, 2021).

$$J = -DA_{\perp}\frac{\partial C}{\partial \lambda} \tag{1}$$

Where J defines the flow of an amount of the chemical species (mass), D represents the concept of diffusivity of the species in the matrix or medium; $A_{\perp}$ represents the surface perpendicular to the flow direction of the species, C is the concentration which corresponds to the dependent variable or of interest of the transfer problem in quantities of mass per unit of volume and, λ can be any dimensional variable concerning a coordinate system. In such a way, the amount of flow is directly proportional to the difference in concentration of the species concerning two positions interconnected by the continuous medium of the matrix, whose homogeneity depends on the capacity factor or mechanism of mobility accounted for through a surface.

In general, the flow balance equation (see **Equation 2**) defined for the domain of a differential volume of the matrix, establishes that the subtraction of the mass flow that enters J_E and leaves J_s through their boundaries or dimensional limits and the mass per unit of volume in which chemical reactions experience transformations, J_T is equivalent to the mass that accumulates of the species in a unit of time J_A.

$$[J_E - J_s] + J_T = J_A \tag{2}$$

Equation 3 results by writing **Equation 2** in differential form, considering three dimensions in a cylindrical coordinate system.

$$-\left[\frac{1}{r}\frac{\partial}{\partial r}\left(-Dr\frac{\partial C}{\partial r}\right)+\frac{1}{r}\frac{\partial}{\partial \theta}\left(-D\frac{1}{r}\frac{\partial C}{\partial \theta}\right)+\frac{\partial}{\partial z}\left(-D\frac{\partial C}{\partial z}\right)\right]+\dot{r}=\frac{\partial C}{\partial t} \tag{3}$$

The nonlinearity characteristic of **Equation 3** and its boundary conditions do not allow mathematical treatment to obtain analytical solutions. Cases in which D cannot be considered constant increase the complexity even further.

ISSN: 2410-3993

Alternatively, the systems are discretized, and numerical solution techniques, such as the finite difference or finite elements, are implemented. In this process, the systems under analysis are subdivided into many subsystems (discrete systems). Differential analysis is transformed into a series of algebraic equations with approximations that depend on the magnitude of the spatial parameters to evaluate the concentration variable (field variable).

In the new discrete scale, the concentration difference in a space interval or gradient is governed by **Equation 4**.

$$\frac{dC}{dx} \cong \frac{\Delta C}{\Delta x} = \frac{C_{x+\Delta x} - C_x}{(x+\Delta x) - x} = \frac{C_{x+\Delta x} - C_x}{\Delta x} \qquad (4)$$

Similarly, **Equation 5** specifies the rate of change concerning time.

$$\frac{dC}{dt} \cong \frac{\Delta C}{\Delta t} = \frac{C^{t+\Delta t} - C^t}{(t+\Delta t) - t} = \frac{C^{t+\Delta t} - C^t}{\Delta t} \qquad (5)$$

By deduction from **Equations 4 and 5**, the smaller the magnitudes of the corresponding intervals, the greater the approximation to the solution of the differential equation. In this sense, the precision of the solution of the numerical analysis by finite differences depends strongly on a correct discretization.

Case study

In the thermochemical carburizing treatment, the objective is to increase the carbon concentration in a region adjacent to the surface of a part (layer), just as swords were in ancient times, and currently, a wide variety of components used for the formation of vehicles, as well as other applications. Typically, the metallographic preparation technique can detect the carburized layer and correlate with processing parameters. Similarly, the results of calculations of carbon transport in steel structures can also be validated with at least two decimal places of precision.

This work presents a methodological structure for developing the fundamental analysis of carburization by solving the transportation problem and its association with a low-cost, reproducible experimental procedure.

The validation method will be limited to assessing the quantification of the ferrite and cementite phases and the pearlite microconstituent (which implies a carbon content) using optical microscopy of samples of an SAE 1018 steel bar.

Methodology

The development of the following methodology was proposed:

1) Formulate the partial differential equation governing the problem of diffusion of the chemical species carbon in iron.

2) Pose the discrete solution problem using the finite difference technique and solve the resulting matrix of the system of algebraic equations using the Thomas algorithm.

3) Use the Microsoft Visual Studio Express platform to code the solution algorithm of the system of equations in the Visual C# language.

4) Carburize 1-inch Ø steel bar samples using pulverized charcoal ($C_{16}H_{10}O_2$) as a carbon “donor”. In the procedure, a chamber made of steel plate sealed with refractory mortar was used to prevent excess oxygen from flowing inside. The box was heated to 950°C inside a muffle furnace and held for nine hours before being slowly cooled inside the furnace out of operation.

5) Perform the analysis of the treated samples using optical microscopy, quantifying the percentage of carbon that causes the distribution of the ferrite phase and the pearlite microconstituent identified, and then compare against the results calculated with the algorithm.

Due to the geometric characteristics of the steel sample, the mathematical formulation of the carburization problem, **Equation 3**, was simplified to one dimension in the radial direction. Also, the chemical reaction of Fe3C formation does not participate in the analysis because it is a component of the pearlite microconstituent. Therefore, by eliminating terms from **Equation 3**, **Equation 6** is formulated.

ISSN: 2410-3993

$$\frac{1}{r}\frac{\partial}{\partial r}\left(Dr\frac{\partial C}{\partial r}\right)=\frac{\partial C}{\partial t} \quad (6)$$

The diagram in **Figure 1** represents a transverse plane of the discretized bar, specifically with three control volumes, where the circle with a solid line defines the edge of the sample. Therefore, the circles with a segmented line define the virtual borders of the subdomains and the points or nodes, their dimensional reference centers.

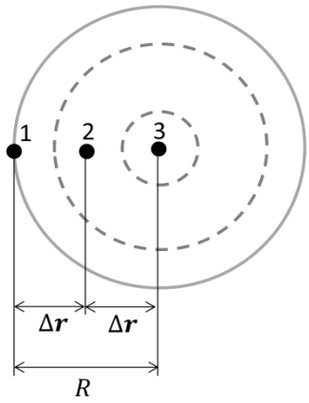

Figure 1 Scheme of the discretization of the geometric model of the cylinder
Source: Own creation in Microsoft PowerPoint 2016

As **Figure 1** dictates, points 1 and 3 define the two physical boundaries for the solution of **Equation 6**. In addition, an initial condition is needed to obtain a particular solution.

Equations 7 to 8 define the two boundary conditions: 1) the condition of the interaction of the solid with its environment and 2) the condition at the central (axial) axis of the cylinder. While **Equation 9** defines the starting state or at time zero for the transient analysis.

$$-D\frac{\partial C}{\partial r}=f, \qquad f=C_b, \qquad r=R \quad (7)$$

$$-D\frac{\partial C}{\partial r}=0, \qquad r=0 \quad (8)$$

$$C(r)=C_0, \qquad t=0 \quad (9)$$

The function f in **Equation 7** was limited to the definition of a constant concentration value. However, it can be more complex.

Fundamentally, for the numerical analysis, the three control volumes determined the representative equations of the entire domain (one for each border and the third according to the geometric pattern between them). In this way, **Equations 6 to 9** were transformed using **Equations 2, 4, and 5**. As a result, after a brief arithmetic development, **Equations 10, 11, and 12** were obtained.

$$C_1^t=C_1^{t+\Delta t} \quad (10)$$

$$\left(\frac{\overline{D_{1\to2}}A_\perp\Delta t}{\Delta r}\right)C_1^t+\left(1-\frac{\overline{D_{2\to3}}A_\perp\Delta t}{\Delta r}-\frac{\overline{D_{1\to2}}A_\perp\Delta t}{\Delta r}\right)C_2^t+\left(\frac{\overline{D_{2\to3}}A_\perp\Delta t}{\Delta r}\right)C_3^t=C_2^{t+\Delta t} \quad (11)$$

$$\left(\frac{\overline{D_{2\to3}}A_\perp\Delta t}{\Delta r}\right)C_2^t+\left(1-\frac{\overline{D_{2\to3}}A_\perp\Delta t}{\Delta r}\right)C_3^t=C_3^{t+\Delta t} \quad (12)$$

Equation 11 is multiplied based on the number of control volumes the user determines to achieve the highest precision in a calculation. Generally, all algebraic equations adopt the structure of **Equation 13**.

$$a_iC_{i-1}^t+b_iC_i^t+c_iC_{i+1}^t=C_i^{t+\Delta t} \quad (13)$$

a, b, c, y, d, represent the respective factors or coefficients of **Equations 10, 11, and 12**. Thus, by proposing an open criterion for specifying the number of control volumes (n), the system of equations represented in matrix form in **Equation 14** was generated, whose explicit solution depends on the calculation time step Δt. The determination of this parameter, called stability criterion, was obtained considering each of **Equations 11 and 12** coefficients, having to satisfy the inequality of being greater – equal to zero, as determined by **Equations 15 and 16** for **Equation 11**, and subsequently detecting the magnitude of the slightest value, which is considered the maximum calculation step.

$$\begin{bmatrix} b_1 & c_1 & \cdots & 0 & 0 \\ a_2 & b_2 & c_2 & 0 & 0 \\ \vdots & \ddots & \ddots & \ddots & \vdots \\ 0 & 0 & a_{n-1} & b_{n-1} & c_{n-1} \\ 0 & 0 & \cdots & a_n & b_n \end{bmatrix}\begin{bmatrix} C_1^t \\ C_1^t \\ \vdots \\ C_{n-1}^t \\ C_n^t \end{bmatrix}=\begin{bmatrix} C_1^{t+\Delta t} \\ C_2^{t+\Delta t} \\ \vdots \\ C_{n-1}^{t+\Delta t} \\ C_n^{t+\Delta t} \end{bmatrix} \quad (14)$$

$$\Delta t\leq\frac{1}{\left(\frac{A_\perp\overline{D_{l-1\to l}}}{\Delta r}\right)}, \qquad \Delta t\leq\frac{1}{\left(\frac{A_\perp\overline{D_{l\to l+1}}}{\Delta r}\right)} \quad (15)$$

ISSN: 2410-3993

$$\Delta t \leq \frac{1}{\left(\frac{A_{\perp}\overline{D_{i\rightarrow i+1}} + A_{\perp}\overline{D_{i-1\rightarrow i}}}{\Delta r}\right)} \quad (16)$$

In turn, the diffusion coefficients were calculated with **Equation 17** and the data table in **Figure 2** and extracted from (Askeland, 2010).

$$D = D_0 exp\left(\frac{-Q}{RT}\right) \quad (17)$$

TABLE 5-1 ■ *Diffusion data for selected materials*

Diffusion Couple	Q (cal/mol)	D_0 (cm^2/s)
Interstitial diffusion:		
C in FCC iron	32,900	0.23
C in BCC iron	20,900	0.011
N in FCC iron	34,600	0.0034
N in BCC iron	18,300	0.0047
H in FCC iron	10,300	0.0063
H in BCC iron	3,600	0.0012
Self-diffusion (vacancy diffusion):		
Pb in FCC Pb	25,900	1.27
Al in FCC Al	32,200	0.10
Cu in FCC Cu	49,300	0.36
Fe in FCC Fe	66,700	0.65
Zn in HCP Zn	21,800	0.1
Mg in HCP Mg	32,200	1.0
Fe in BCC Fe	58,900	4.1
W in BCC W	143,300	1.88
Si in Si (covalent)	110,000	1800.0
C in C (covalent)	163,000	5.0
Heterogeneous diffusion (vacancy diffusion):		
Ni in Cu	57,900	2.3
Cu in Ni	61,500	0.65
Zn in Cu	43,900	0.78
Ni in FCC iron	64,000	4.1
Au in Ag	45,500	0.26
Ag in Au	40,200	0.072
Al in Cu	39,500	0.045
Al in Al_2O_3	114,000	28.0
O in Al_2O_3	152,000	1900.0
Mg in MgO	79,000	0.249
O in MgO	82,100	0.000043

Data from several sources, including Adda, Y. and Philibert, J., La Diffusion dans les Solides, Vol. 2, 1966.

Figure 2 Table of thermodynamic data for determining the diffusion of a couple of chemical species
Source: Image obtained from (Askeland, 2010).

The temperature T corresponds to the conditions of the thermal index reached during carburization (950 °C), and R represents the universal gas constant.

Equations 18 and 19 define the sequence of the Thomas algorithm for the solution of the matrix system of **Equation 14**.

$$c'_i = \begin{cases} \frac{c_i}{b_i}; & i = 1 \\ \frac{c_i}{b_i - c'_{i-1}a_i}; & i = 2,3,\dots,n-1 \end{cases}$$

$$d'_i = \begin{cases} \frac{d_i}{b_i}; & i = 1 \\ \frac{d_i - d'_{i-1}a_i}{b_i - c'_{i-1}a_i}; & i = 2,3,\dots,n \end{cases} \quad (18)$$

$$C_n = d'_n$$
$$C_i = d'_i - c'_i C_{i+1};\ \ i = n-1, n-2, \dots, 1 \quad (19)$$

Therefore, the pseudocode presented in **Figure 3** defines the general calculation algorithm.

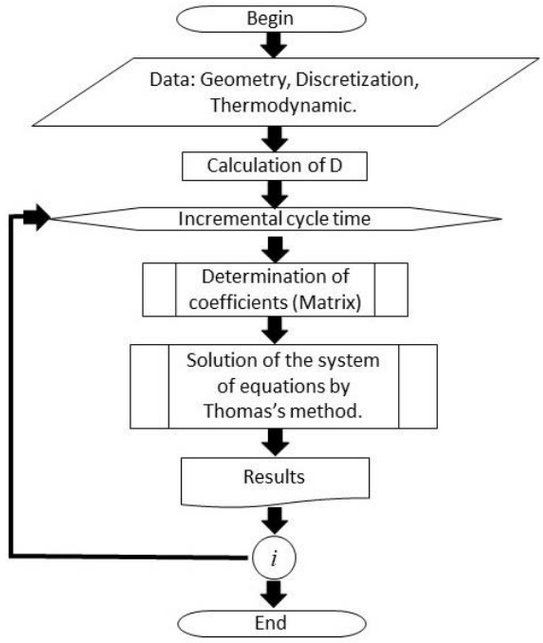

Figure 3 Flow chart for the development of computer programming
Source: Own creation in Microsoft PowerPoint 2016.

Figure 4 shows the graphical user interface developed in the Visual C# language for data entry and presentation. Calculations of carbon concentration histories and profiles will be tabulated in a table (middle) and plotted in a scatter plot when selecting some set for trend analysis (right).

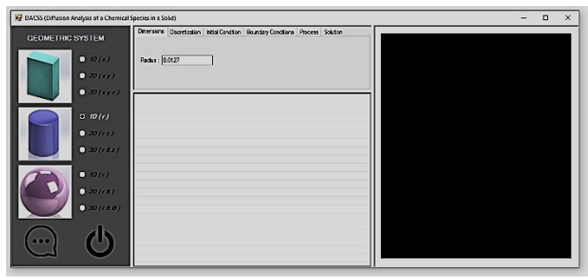

Figure 4 Graphical user interface developed for calculating carbon concentration histories and profiles in the carburization process
Source: Image by screenshot of the development in MS Visual Studio Express 2010.

ISSN: 2410-3993

The carburization process involves the calculation of carbon concentration histories and profiles. This includes the preparation of charcoal powder inside a metal box, which is then sealed and introduced into the muffle furnace (Nabertherm, 2023). The process is shown in **Figures 5(a) and 5(b)**.

(a)

(b)

Figure 5 Experimental procedure: a) metal box containing the charcoal powder and the test sample, b) sealed box introduced into the muffle furnace
Source: Own photographs. Metallurgy laboratory.

To analyze the phase distribution of untreated and treated samples, optical microscopy analysis is conducted at 10X. The surfaces are etched with 3% Nital for 5 seconds, as shown in the micrograph of **Figure 6**.

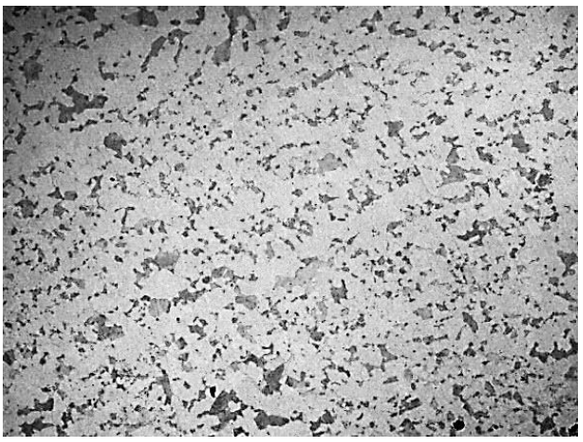

Figure 6 Micrograph obtained at 10X of the preparation of the original SAE 1018 steel specimen, etched with 3% Nital for 5 s
Source: Own image (PAX-it!, 2022).

Figure 7 is a diagram of the Fe-C predominance or metastable equilibrium, with the marking of the composition for the formation of one hundred percent pearlite (vertical line segmented at 0.77%), as well as the partition for the application of the lever rule (solid line and dot, red color). The dot indicates the average 0.20 weight percent C composition of SAE 1018 steel.

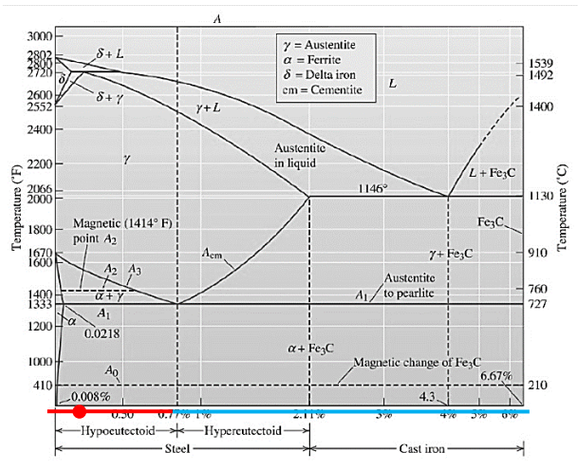

Figure 7 Metastable predominance diagram of the Fe-C system
Source: Image obtained from (Askeland, 2010).

The lever rule equations for determining the percentage of ferrite (%α), cementite (%Fe3C), and the percentage of pearlite (%P), as a function of the C content in the Fe-C diagram, are defined in **Equations 20 and 21** according to (Avner, 1982).

$$\%\alpha = \left(\frac{0.77 - \%C}{0.77 - 0.008}\right)100 \qquad (20)$$

ISSN: 2410-3993

$$\%P = \left(\frac{\%C - 0.08}{0.77 - 0.008}\right)100 \quad (21)$$

Substituting 0.2 into **Equations 20 and 21** generates 74.8 %α and 25.2 %P values. Therefore, this defines the phase (light zone) and microconstituent (shaded zones) distribution in the micrograph of **Figure 6**. In turn, if the lever were to change to the blue line marked in **Figure 7**, the distribution of the Fe_3C cementite phase and the pearlite microconstituent is obtained through **Equations 22 and 23**, which is adopted when determining the initial concentration of carbon exceeds 0.77% by weight.

$$\%P = \left(\frac{6.7 - \%C}{6.7 - 0.77}\right)100 \quad (22)$$

$$\%Fe_3C = \left(\frac{\%C - 0.77}{6.7 - 0.77}\right)100 \quad (23)$$

Results

The microstructure obtained in the steel specimen evolves under conditions close to those dictated by the metastable Fe-C equilibrium diagram. The micrograph of **Figure 8** shows the microstructure obtained after metallographic preparation in a cross-section of the treated specimen. Notice a significant difference between the micrographs of **Figure 6 and Figure 8**. The 10X field of view allows showing just over 2 mm of surface from the edge of the specimen. The microstructure analysis determined the existence of 100% pearlite in the region just over 1 mm deep.

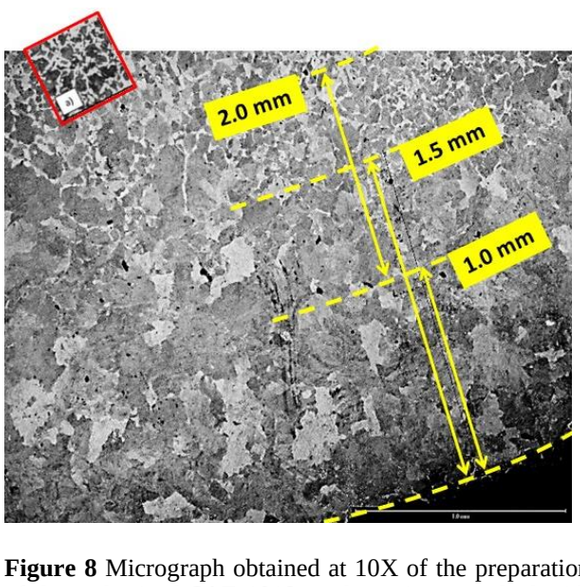

Figure 8 Micrograph obtained at 10X of the preparation of the carburized SAE 1018 steel specimen, etched with 3% Nital for 5 s
Source: Own image (PAX-it!, 2022)

The coexistence of pearlite and the cementite phase (free Fe_3C) appears before the 1 mm mark. Cementite precipitated at the grain boundary and on small, barely noticeable islands (with a decreasing distribution from the edge to the mark). Consequently, above the 1 mm mark, a distribution of the ferrite phase and the pearlite microconstituent was found.

It was necessary to obtain a percentage valuation of the ferrite and cementite phases and the pearlite microconstituent in each position relative to the marks in the micrograph of **Figure 8** to quantify the percentages of carbon clearing from **Equations 20, 21, 22, and 23**. **Table 1** summarizes the determination of ferrite and pearlite percentages based on the distribution of the ferrite and cementite phases concerning the limit of the 100% pearlite content (0.77%C).

#	Mark mm	%α	%Fe_3C	%P	%C
1	0	0	5	95	1.06
2	0.5	0	2	98	0.89
3	1	0	1	99	0.75
4	1.5	20	0	85	0.61
5	2	35	0	65	0.50
6	2.2	42	0	58	0.45

Table 1 Ferrite and pearlite percentage data associated with the carbon concentration at a point on the lines drawn in the modified microstructural region of sample A

The red framed box in **Figure 8** represents a micrograph obtained from an SAE 1045 steel (0.45% C). Given the similarity with the background microstructure, near the 2.2 mm distance, the corresponding distribution of 42%α, 58%P can be associated with the tested specimen. On the other hand, **Figure 9** shows a screenshot of the calculations obtained by solving **Equations 6 to 9**.

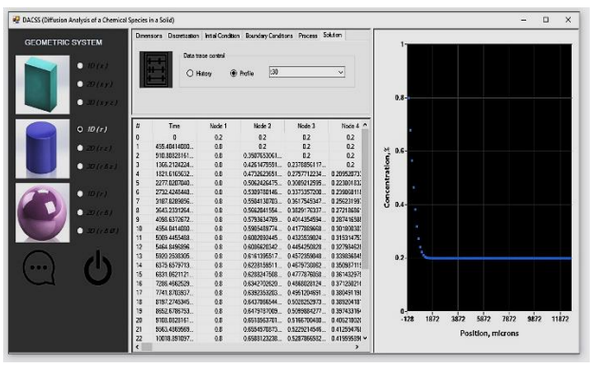

Figure 9 Developmental graphical user interface for calculating carbon concentration histories and profiles in the carburization process
Source: Image by screenshot of the development in MS Visual Studio Express 2010

ISSN: 2410-3993

The developmental graphical user interface for calculating carbon concentration histories and profiles in the carburization process is shown in **Figure 9**. It was possible to obtain the value of the diffusion coefficient [$D = 3.039E-11\ m^2s^{-1}$] for calculations with the application using **Equation 17** and the parameters obtained from the table in **Figure 2** [$Q = 32900\ cal\ mol^{-1}$ $Do = 0.23\ cm^2\ s^{-1}$]. As well as considering a process temperature value T=1223.15 K. Additionally, a constant value of the concentration of carbon percent in the boundary condition $r = R$ of $C_b = 1.06$ (refer to **Equation 7**), a constant value of the concentration of initial of carbon percent in the steel $C_0 = 0.2$ (refer to **Equation 9**). Finally, a homogeneous discretization considering 99 control volumes and two processing times, 9 and 12 hours.

Graphic 1 shows the results of the %C calculation according to 1) the experimental estimates tabulated in **Table 1** (filled circles) and 2) the data calculated from the concentration field by mathematical modeling for 9 and 12 hours of process (lines segmented and dotted, respectively).

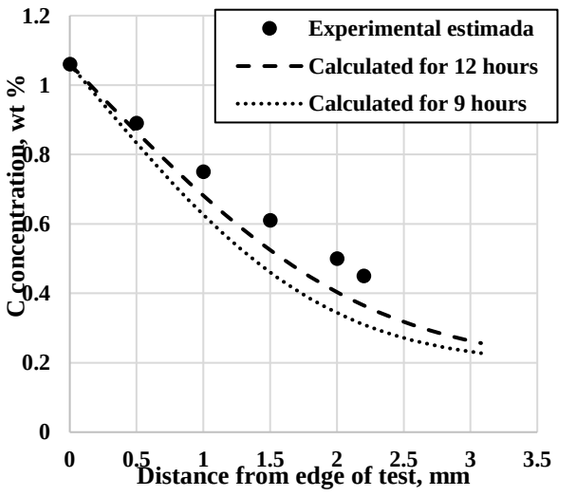

Graphic 1 Carbon concentration profiles in the carburization process were estimated experimentally (filled circles) and calculated with the mathematical model (dotted and segmented lines). *Own creation in Microsoft Excel 2016.*

The graphcis of the curves show that the calculations with the mathematical model and the experimental estimation differ more when establishing profiles with 9 hours of holding in the oven at 950 °C (dotted line).

However, suppose three hours to consider that diffusion originated and continued during the heating and cooling ramps. In that case, the calculation fits much better with the experimental determination. In this sense, the application can help adjust these offsets by correlating the solution to some of the predefined parameters.

On the other hand, the appreciation of the distribution of the ferrite phase and the pearlite microconstituent may also be overestimated in the micrographic analysis since the analyst's judgment is implicit.

Thanks

The authors thank the Tecnológico Nacional de México, which, through the Instituto Tecnológico de Morelia, provided financial support for the publication of this material.

Conclusions

The validation of the transport model of chemical species determines that the estimated diffusion is well determined considering the existence of the phase with high solubility at high temperature (austenite) of the Fe-C system.

However, appreciating the phase distribution under qualitative equilibrium conditions is not a well-founded reference since it depends on the analyst. A best practice for comparing information should be based on an analysis of carbon concentration obtained with specialized chemical analysis equipment, such as an X-ray energy dispersive (fluorescence) elemental analyzer that can be fitted to a scanning electron microscope (SEM).

The computer application generates results effectively, and the parameters entered to obtain various calculations are easily redefined, mainly to adjust equivalent process times that include the effect on the diffusion of the heating and cooling ramps. Furthermore, if accurate indicator measurements were available during the process, more complex models could be implemented to define new diffusion coefficient data and a more complex sample surface boundary condition.

ISSN: 2410-3993

Additionally, the application would not only be limited to the carburization process since the same phenomenology governs other processes of similar interest. Therefore, computational development can be used for any system where the diffusion of chemical species is the phenomenon of interest.

References

Askeland, D. R. (2010). *The Science and Engineering of Materials (6a ed.--.).* Australia, Brazil, Japan, Korea, Mexico, Singapore, Spain, United Kingdom, United States: Cengage Learning.

Avner, S. H. (1982). *Introduction to Physical Metallurgy.* Tokyo: Mc Graw-Hill International Book Company.

Crank, J. (1975). *The Mathematics of Diffusion.* Glasgow, New York, Toronto, Melbourne, Wellington, Cape Town, Ibadan, Nairobi, Dar es Salaam, Lusaka, Addis, Ababa, Delhi, Bombay, Calcutta, Madras, Karachi, Lahore, Dacca, Kuala Lumpur, Singapore, Hong Kong, Tokyo: Clarendon Press - Oxford.

Edenhofer, B., Joritz, D., Rink, M., & Voges, K. (2015). Carburizing of Steels. In M. A. Eric J. Mittemeijer, *Thermochemical Surface Engineering of Steels* (pp. 485-553). Kleve, Germany: Woodhead Publishing. https://doi.org/10.1533/9780857096524.3.485

Goldstein, J. M. (1978). Diffusion modeling of the carburization process. *Metall Trans A, 9*, 1515-1525. https://doi.org/10.1007/BF02661934

Grabke, H. J. (2002). Carburization, carbide formation, metal dusting, coking. *Materiali in tehnologije, 36*(6), 297-306.

Grabke, H., & Wolf, I. (1987). Carburization and oxidation. *Materials Science and Engineering, 87*, 23-33. doi.org/10.1016/0025-5416(87)90357-0

Lee, S.-J., Matlock, D. K., & Van Tyne, C. J. (2013). Comparison of two finite element simulation codes used to model the carburizing. *Computational Materials Science*, 47-54. http://dx.doi.org/10.1016/j.commatsci.2012.10.007

Nabertherm. (2023). *Furnaces for Foundry.* Lilienthal, Germany: Nabertherm GmbH. Retrieved from https://www.nabertherm.com/contacts

PAX-it! (2022). *PAX-it! Image Management, Measurement, and Analysis*. Retrieved from PAX-it!: https://www.paxit.com/

Porter, D. A. (2021). *Phase transformations in metals and alloys.* Abingdon, Oxon: CRC press.

Rahmel, A., Grabke, H. J., & Steinkusch, W. (1998). Carburization - Introductory Survey. *Materials and Corrosion*, 221-225.

ISSN: 2410-3993